ADVANCED ENERGY MATERIALS
www.advenergymat.de

Dual Optimization of Bulk and Surface via Guanidine Halide for Efficient and Stable 2D/3D Hybrid Perovskite Solar Cells

Xiaobo Zhang, Wencai Zhou, Xiaoqing Chen, Yichuan Chen, Xuhong Li, Manqi Wang, Ying Zhou, Hui Yan, Zilong Zheng,* and Yongzhe Zhang**

In order to improve both performance and stability of perovskite solar cells, a design is provided by combining the advantages of high-efficiency 3D perovskite solar cells (PSCs) and long-term stability 2D PSCs. A 2D/3D hybrid perovskite film with a dual (bulk- and surface-) passivation approach is realized, based on in-depth discussion of the guanidine halide (GuX) passivation mechanisms. The approach can reduce the charge carrier losses in the bulk and prevent decomposition at the surface. Based on a combination of ab initio molecular dynamics simulations, Urbach energy, and photovoltage measurements, it is indicated that the engineered components of GuX salts are GuCl for bulk treatment and GuI surface treatment, respectively. The former can lower the nonradiative recombination, and the latter can prevent the halogen-out. Moreover, drive-level capacitance profiling is employed in the context of the 2D/3D perovskite structure for revealing and proving the passivation mechanism. The 2D/3D hybrid perovskites achieve long-term stability (efficiency degradation <10% after 30 days without encapsulation) and significant enhanced efficiency (22.53%) compared with the efficiency (20.31%) of the control device. This work represents a rational design strategy for bulk and surface passivation treatment in 2D/3D hybrid perovskites.

1. Introduction

Since its first emergence in 2009 with a power conversion efficiency (PCE) of 3.8%,[1] Organic–inorganic perovskite solar cells (PSCs) have undergone an unprecedented rapid development, reaching the present certified PCE record at 25.7%.[2]

To further improve the PCE and stability of PSCs, we need to suppress the free carrier losses in the perovskite bulk and improve the hydrophobicity of the perovskite surface. For this purpose, many methods have been efficiently utilized, including bulk passivation (e.g., composition engineering via excess PbI_2 in situ growth[3]) and surface passivation (e.g., capping with 2D perovskite capping[4–8] or other organic materials like poly(methyl methacrylate) and phenyl-C_{61}-butyric acid methyl ester (PCBM)[9,10]).

Among these methods, passivation by quasi-2D perovskite is successfully used in a broad range of optoelectronic applications such as perovskite-based solar cell,[11–13] light emitting diode,[14–16] and detector.[17] In contrast to 3D perovskites, the 2D perovskites with introduction of long-chain organic groups are more thermally stable, hydrophobic, and suppress internal ion migration.[18–21] However, PSCs with pure 2D perovskites are lowered in PCE than those with 3D perovskites because pure 2D perovskites are 1) inefficient in charge transport across the organic interlayer, 2) inefficient in light conversion due to their wider optical bandgap.[18–21] To balance between stability and efficiency, the emerging 2D/3D hybrid PSCs has been regarded as a promising photovoltaic technologies.[8,11,13,22–30]

X. Zhang, W. Zhou, X. Chen, Y. Chen, M. Wang, H. Yan, Z. Zheng, Y. Zhang
College of Material Sciences and Engineering
Beijing University of Technology
Beijing 100124, P. R. China
E-mail: chenxiaoqing@bjut.edu.cn; zilong.zheng@bjut.edu.cn; yzzhang@bjut.edu.cn

X. Chen, Y. Zhang
Key Laboratory of Optoelectronics Technology
College of Microelectronics
Faculty of Information Technology
Beijing University of Technology
Beijing 100124, P. R. China

The ORCID identification number(s) for the author(s) of this article can be found under https://doi.org/10.1002/aenm.202201105.

Y. Chen
School of Mechanical and Electrical Engineering
Jingdezhen Ceramic University
Jingdezhen, Jiangxi 333403, P. R. China

X. Li
School of Physics
Beihang University
Beijing 100191, P. R. China

Y. Zhou
Electronics and Photonics Research Institute
National Institute of Advanced Industrial Science and Technology (AIST)
Tsukuba 3058565, Japan

DOI: 10.1002/aenm.202201105

Recently, a new kind of 2D perovskite based on guanidinium (Gu) passivation has attracted intense interest. A unique advantage is that Gu halide salts (GuX) could be used both in the bulk passivation via incorporating into the 3D perovskite lattice[19] and on the surface passivation via forming 2D capping layer.[31] In the latter condition, a new structure of 2D perovskite (alternating cation in the interlay space, ACI) is formed, which is expected to be a good alternative for the most intensely studied Ruddlesden–Popper 2D perovskite in inter-slab charge transport because of its narrower inter-slab distance and conjugated nature.[32] Because of these merits, GuX allows for bulk-and-surface dual optimization which is promising to simultaneously satisfy the criteria for the bulk treatment and surface treatment. After 3 years of development, the PCE of solar cell based on single Gu-halide-modified PSCs rapidly raised to 22.17%,[33,34] which is however still below the record of solar cell based on 3D perovskite (25.7%[2]). In order to further improve the PCE, GuX should be used along with other optimization techniques (modified charge transport layer[35]) or additives (4-*tert*-butyl-phenylmethylammonium iodide[36]). A prerequisite for reasonably combining these techniques is to understand the improvement mechanisms of GuX, which is not easy because of their versatile roles in the bulk and on the surface. The unclear questions include the respective roles of Gu^+ cations and halide anions, and the respective requirements for bulk doping and surface post-treatment, etc. After these questions are answered, the GuX could be fairly compared with other analogous additives or feasibly used along with other passivation methods.[37–42]

In this work, to address these questions and screen out the most suitable GuX salt for both bulk passivation and surface passivation, we first adopted theoretical calculations to analyze the formation energy of iodine-related defects, quantum dynamic processed of electron-hole non-radiative recombination, and the active energy barrier of interstitial Cl/Br/I anion migration. Next, through systematic experiments, we confirmed that the 2D/3D hybrid perovskite film structure is successfully realized, the defects are successfully passivated and active energy of ion migration is obviously increased. Consequently, the dual passivation optimization leads to a remarkably enhanced performance compared to the control devices, with up to 22.53% PCE, which exhibits an excellent stability with >90% of its initial value under ambient air conditions. Furthermore, our work reveals a rational design strategy for bulk and surface treatment of the perovskite film.

2. Results and Discussion

2.1. Effect of Various GuXs on the Perovskite Bulk and Surface

The criterion for the best GuX bulk dopant is to minimize the nonradiative recombination. The primary contributor to the nonradiative recombination is the Shockley–Read–Hall (SRH) recombination related to the defect density. Because the defect density is determined by its formation energy, the first principles calculations were adopted to study the formation energies of the iodine-related defects (iodine vacancy (V_I)), which is the easiest to form among all the usual defects.[24] The V_I formation energy is defined as the difference in the total crystal energy before and after the V_I arises, which represents the penalty in broken initial atomic bonds and in lattice stress. The optimized perovskite structures incorporating the various GuX are shown in **Figure 1**a, and the calculated formation energies of the V_I for pristine $FAPbI_3$ and $FAPbI_3$ doped with GuCl, GuBr, GuI are 0.73, 0.91, 0.92, and 0.69 eV, respectively. Apparently, the results for formation energy indicate that GuI bulk doping can facilitate the generation of iodine-related defects, while GuCl and GuBr bulk doping are similarly good to suppress this process.

The secondary contributor to the nonradiative recombination is the electron–hole (e–h) non-radiative recombination assisted by phonons as Figure 1b. Our molecular dynamic calculations revealed that the excited state lifetime is GuCl (60.72 ns) > pristine $FAPbI_3$ (54.20 ns) > GuBr (43.61 ns) > GuI (34.72 ns). In particular, the GuBr and GuI doping system accelerate the nonradiative electron-hole recombination, while the GuCl doping system suppresses it compared to the pristine $FAPbI_3$, in which charges relax within tens of nanoseconds, in agreement with the previous reports.[43–45] The long charge carrier lifetimes in GuCl doping system is due to the weak NA coupling and short pure-dephasing/decoherence time.[45] According to our results of the formation energy and excited state lifetime, GuCl doping is expected to be the best bulk doping candidate. (The calculation details are provided in the experimental section and Figures S1 and S2, Supporting Information.)

Distinct with bulk doping, the criterion for the best GuX surface dopant is to form a stable hydrophobic 2D capping layer. Since a major degradation mechanism is the loss of the X^- anions through evaporation,[46] we should maximize the migration activation energy barrier for X^- anions which is determined by the halogen ion size. As Cl^- anion has the smallest ion radius in the candidate GuX species, Cl^- need to overcome the lowest activation energy barrier (0.59 eV) due to steric hindrance effect making it much easier to migrate from perovskite crystal to surface (Figure 1c). On the contrary, I^- anion has the biggest ion radius and highest activation energy barrier (0.73 eV) in the candidate GuX species, implying that GuI can effectively present in the perovskite crystal. Therefore, the GuI is expected to be best in forming a stable hydrophobic 2D perovskite capping layer. (The formation energy of defects after the GuX absorbed on the perovskite surface is in the end of supplementary discussion of simulation results and Figure S3, Supporting Information.)

As suggested by the theoretical calculation results, GuCl bulk doping along with GuI surface post-treatment is the optimal scheme for performance enhancements. Therefore, systematic experiments were carried out to verify these theoretical results. The structure of corresponding PSCs is ITO glass/SnO_2/FA-based mixed perovskite/2D perovskite/Spiro-OMeTAD/Au (**Figure 2**a). The experiment details are provided in the experimental section and Figure S4, Supporting Information. First, we studied the effects of different GuX on the perovskite bulk doping, of which the device statistical PCE is shown in Figure 2b along with the corresponding J_{sc}, V_{oc}, and FF parameters in Figure S5, Supporting Information. Upon the introduction of GuCl, the average PCE (20.07%) is significantly higher than that of GuBr (17.71%) and GuI (18.01%) bulk doping device as well as control device without GuX passivation (18.46%). This PCE increase comes from the variation of recombination lifetime and Urbach energy (E_u). Recombination lifetime was characterized

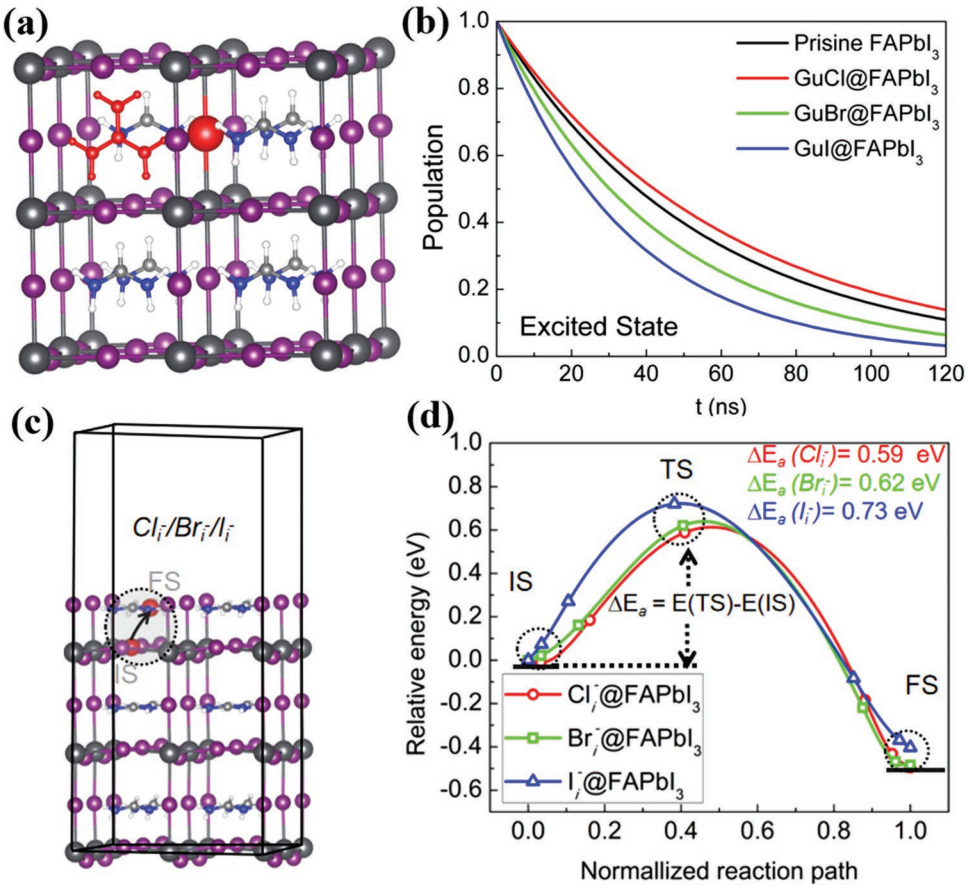

Figure 1. a) Scheme of GuX-doped FAPbI3 in first-principles calculations. b) Population decay of excited states (CBM) in pristine $FAPbI_3$ and GuX-doped $FAPbI_3$ based on Ab-initio molecular dynamics simulations. c) Diagrammatic sketch of halogen ion interstitial ($Cl_i^-/Br_i^-/I_i^-$) migration from perovskite bulk (defined as initial state, IS, which is the reference point of total energy) to surface (defined as final state, FS) along with d) the energy profile. The activation energy barrier is defined as the energy difference between the IS and transition state (TS).

via transient photovoltage (TPV) measurements.[47] As shown in Figure 2c, the recombination lifetime of the control, GuCl, GuBr, and GuI bulk doping device are 0.93, 1.16, 0.66, and 0.72 ms, respectively. The prolonged recombination lifetime could be ascribed to the lowered defect density in the perovskite film.[48] In addition, the lower E_u of the perovskite film indicates a higher structural quality of the film, as well as a lower voltage loss between V_{oc} and the bandgap voltage.[49] Figure 2d shows E_u for the perovskite films calculated from ultraviolet–visible (UV–vis) absorption spectra using the equation $\alpha = \alpha_0 \exp(h\nu/E_u)$, where α is absorption coefficient and $h\nu$ is photon energy.[49] The detailed calculation process is showed in Figure S6, Supporting Information. The E_u of the control, GuCl, GuBr, and GuI bulk doping perovskite films are 93.72, 89.36, 111.21, and 107.16 meV, respectively. Among the different GuX bulk doping, GuCl bulk doping device owns the longest recombination lifetime and lowest E_u, which result in the best performance and implies that the GuCl bulk doping is the best choice, which is consistent with the theoretical calculation results.

On the basis of GuCl bulk doping, we further studied the effects of different GuX on the surface post-treatment between the perovskite and the hole transport layer (HTL), of which the device statistical PCE is shown in Figure 2b. The average PCE of GuCl, GuBr, and GuI surface post-treatment device are 20.97%, 19.31%, and 19.05%, respectively. The highest PCE of GuI surface post-treatment device comes from its longest recombination lifetime and lowest Urbach energy among the candidate GuX species (Figure 2c,d). GuI is optimal because only GuI can be stably conserved at the interface, as suggested by our theoretical calculations.

Based on the above theoretical and experimental results, the best dual optimization scheme is GuCl bulk doping and GuI surface post-treatment. In order to further deepen the understanding of the respective roles of bulk and surface passivation, we carried out comparative studies on devices based on three types of perovskite layers, namely, 1) pristine perovskite layer (control), 2) perovskite layer with solely GuCl bulk passivation (3D), 3) perovskite layer with both GuCl bulk doping and GuI surface post-treatment (2D/3D). In the following, we will sequentially confirm 1) the device performance improvement, 2) the 2D/3D hybrid structure, and 3) the defect passivation.

2.2. The Device Performance Improvement

The champion performances of three types of devices are shown in **Figure 3**a. The control device based on the pristine perovskite

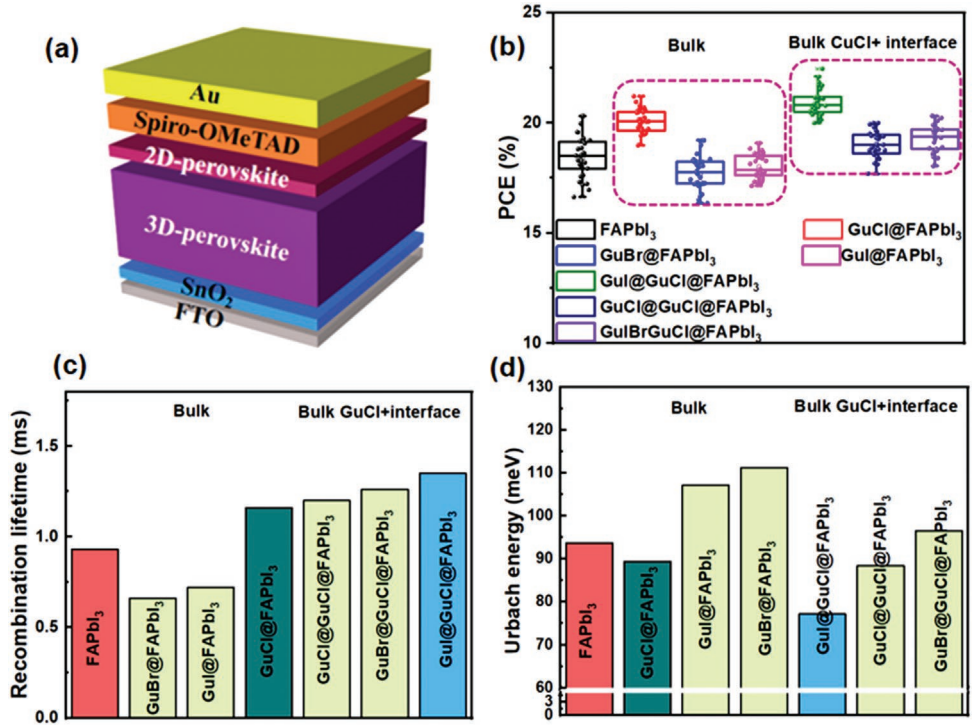

Figure 2. a) The schematic of PSCs with n-i-p configuration based on 2D/3D perovskite heterojunction with guanidine halide treatment. b) The statistical PCE for devices with the various GuX treatment. c) Recombination lifetime of different GuX modified devices, characterized via transient photovoltage measurements. d) Urbach energy of different GuX modified perovskite films, calculated from UV–vis absorption spectra.

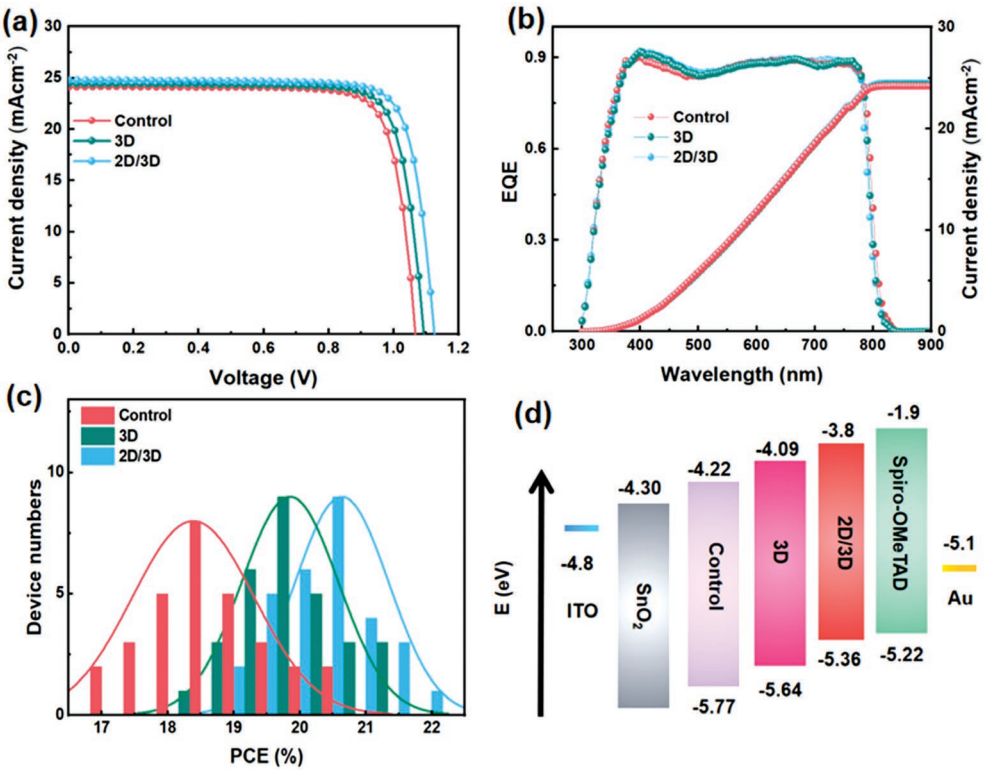

Figure 3. a) Current density–voltage curves for all samples. b) External quantum efficiency for all samples. c) The device PCE distribution for all samples; 30 devices data are collected for each type of device. d) The band energy diagram of three PSCs.

shows a maximum PCE of 20.31%, with a V_{oc} of 1.06 V, the J_{sc} of 24.16 mA cm^{-2} and the FF of 78.32%. In comparison, the 3D device based on the perovskite incorporated with GuCl shows an improved PCE of 21.56%, with a V_{oc} of 1.09 V, J_{sc} of 24.41 mA cm^{-2}, and an FF of 81.03%. Moreover, the 2D/3D device based on the perovskite with the GuCl doping and GuI surface post-treatment exhibits the highest efficiency and negligible hysteresis (Figure S7, Supporting Information), with a maximum PCE up to 22.53%, a V_{oc} of 1.12 V, an J_{sc} of 24.79 mA cm^{-2}, and an FF of 81.15%. The integrated J_{sc} from the external quantum efficiency (EQE) measurement for the control, 3D, and 2D/3D device are 24.08, 24.32, and 24.45 mA cm^{-2}, respectively (Figure 3b), which are consistent with those measured from J–V curves. The increased J_{sc} comes from the absorption enhancement in the short-wave range (300–500 nm), which was also confirmed by the UV–vis absorption spectra (Figure S8a, Supporting Information). In Figure 3c, the statistic PCE results (30 devices of each type) show the guanidine halide treatment can obviously improve the average PCE from 18.5% to 19.7% and 20.5%. The steady-state power outputs for 200 s measured under the maximum power points is 21.11% for the champion devices (Figure S9, Supporting Information). To further understand the mechanism of photovoltaic performance improvement, ultraviolet photoelectron spectroscopy (UPS) measurement was performed to investigate the band energy diagram of three PSCs (Figure S10 and Table S2, Supporting Information). As shown in Figure 2d, upshifted E_{VB} of film 3D and 2D/3D as compared to film control can form a gradient energy alignment, which is beneficial for reducing potential difference between perovskite and hole transport layer.[50,51] Meanwhile, the upshifted E_{CB} can inhibit electron-hole recombination at the perovskite/HTL interface, where the electron from the conduction band perovskite exist potential recombination with the hole from the value band of spiro-OMeTAD.[31] In order to determine the dynamics of charge transfer and extraction at the interface, steady-state photoluminescence (PL) was performed, based on the different device architecture. As shown in Figure S8a, Supporting Information, the slight shifts can be found with the PL emission peaks at 805, 803, and 799 nm for control, 3D, and 2D/3D, respectively, which is consistent with the absorption spectra. Moreover, compared with the control devices, 3D, and 2D/3D devices show a stronger PL quenching effect. It indicates when GuCl and GuI are employed as a passivant at the bulk and surface of perovskite can accelerate carrier extraction from perovskite to spiro-OMeTAD, coming from the gradient energy level.

2.3. The 2D/3D Hybrid Structure

In this section, we will confirm the 2D/3D hybrid film structure, namely, the GuCl bulk incorporation plus the GuI surface capping. The hybrid structure was confirmed by photoluminescence (PL), X-ray diffraction (XRD), microstructure characterization, and the corresponding electron diffraction (selected area electron diffraction, SAED, nano-beam electron diffraction, NBD) from the aspects of optical, crystal, and microscopic properties.

First, top-view SEM was measured to study the effect of guanidine halide on the grain size and surface morphology as shown in **Figure 4**a. While all films showed similar surface morphology with cross-linked grains and no apparent pinholes, the surface texture of the 2D/3D perovskite film is different. The AFM results confirmed that the root mean square roughness of 2D/3D perovskite film is reduced (Figure 4b). A possible reason is that the GuI reacted with the lead iodide, leading to successful formation of a 2D perovskite capping.[7] In addition, we find that GuCl, GuBr, and GuI doping can all facilitate the growth of grain size, and GuCl doping has the most positive effect (Figure S11, Supporting Information). Therefore, crystal growth kinetics is assumed to be controlled by both Gu^+ and Cl^- via an underlying interaction of GuCl with PbI_2 and/or $FAPbI_3$. Compared with FA^+, Gu^+, as a type of Lewis acid and owning more abundant ammonium group, can enhance the interaction of GuCl with PbI_2 and/or $FAPbI_3$, which then is in part responsible for the enlarged grain size and surface uniformity.[13,52,53] Meanwhile, the chloride ion, which has a similarly positive effect to facilitate the growth of grain size, is a widely used additive used to improve the crystallinity of perovskite films, which consequently reduce defect state density.[54,55]

To confirm the presence of 2D perovskite on the perovskite top surface, we performed the steady PL for the 2D/3D film with different incident excitation light directions (Figure S8c, Supporting Information) when the excited light comes from the top or bottom (perovskite film or glass) side. Compared with the excitation light from the glass side, when excitation light from the perovskite side, the PL peak exist an obvious blue shift, which contribute from a newly formed wide band-gap perovskite on the film top surface. However, whether this wide band-gap perovskite belongs to 2D perovskite needs further characterization. In addition, we also measured the PL-mapping as Figure S12, Supporting Information, which shows much more intense and uniform in the 2D/3D perovskite film compared with the control and 3D perovskite film. The strong PL enhancement in 3D and 2D/3D perovskite film indicates that guanidine halide treatment can suppress the SRH recombination and e–h non-radiative recombination.[56]

Next, XRD was performed to characterize crystal structures of the above-mentioned wide band-gap perovskite. As illustrated in Figure S13a, Supporting Information, the peak at 14° slightly shifts to lower angle after guanidine halide treatment, indicating the expansion of the crystal lattice due to incorporation of the large guanidine cation (Figure S13b, Supporting Information).[57] We notice that an additional peak at ≈11° is found only in the 2D/3D perovskite film, which could be attributed to either the δ-$FAPbI_3$ or the Gu_2PbI_4 2D perovskite phase. In addition, lattice strain result indicates, when the appropriate doping contraction incorporated in $FAPbI_3$, the lowest strain appeared (Figure S14, Supporting Information). Thus, composition engineering by incorporating the large cations Gu^+ has been introduced to modulate the lattice tensile strain toward minimizing defect centers or traps that can capture charge carriers and enhancing the intrinsic stability of perovskite films.[12,58]

In order to further clarify the nature of the peak around 11°, the grazing incident XRD (GIXRD) with 0.5° incident angle characterization which is selectively sensitive to the film surface was employed. As shown by Figure S13c, Supporting Information, the PbI_2 peak is present in the pristine and 3D films but absent in the 2D/3D film. This result indicates that on the 2D/3D film, the excessive PbI_2 reacted with the introduced GuI

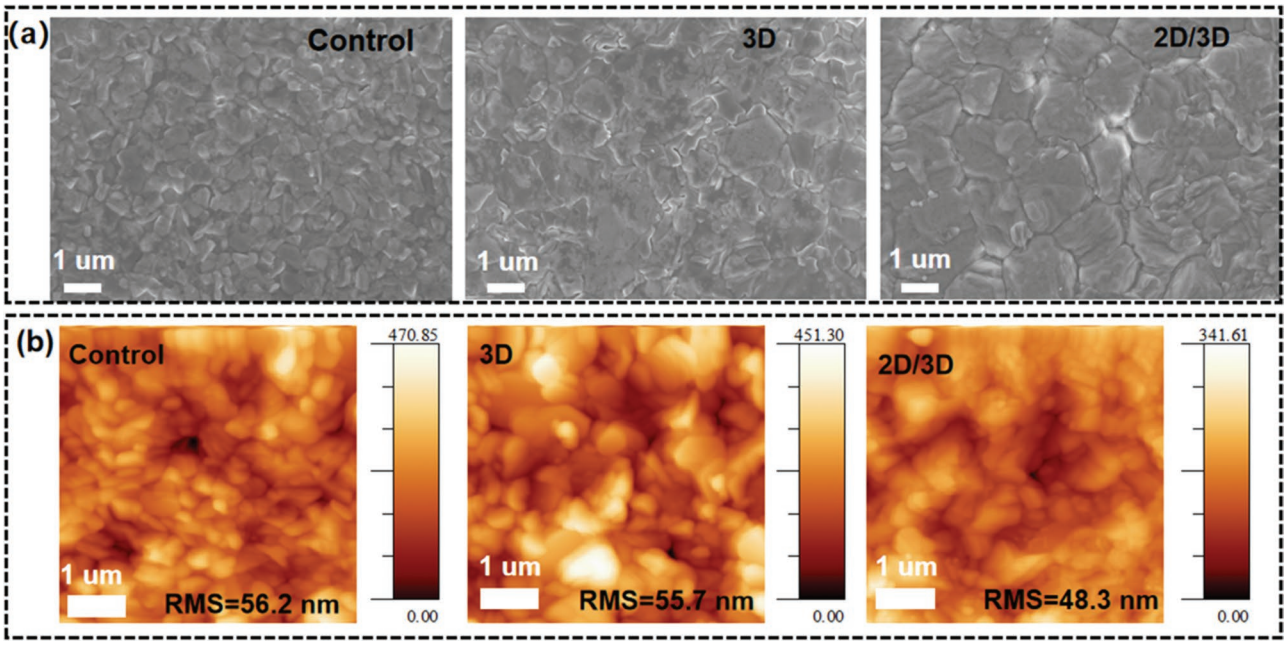

Figure 4. Top view SEM images (a) and AFM images (b).

on the perovskite top surface. Therefore, we suspect the possibility of δ-$FAPbI_3$ may be ruled out because Gu^+ is not involved. In addition, the obvious diffraction peak around 11° is only found in the 2D/3D film (Figure S13d), which suggests that Gu_2PbI_4 only exist in the 2D/3D film.[31]

To further confirm the 2D perovskite formed on the surface of 3D perovskite, GIWAXS has been carried out. As shown in **Figure 5**a–c, only diffraction signals corresponding to the 3D perovskite (q = 10.2 nm^{-1}) and excess PbI_2 (q = 9.1 nm^{-1}) are identified for the control and 3D films, which are consistent with the XRD results. The difference between control and 3D films (Figure 5a,b) is that the peak intensity belonging to PbI_2 (3D perovskite) significantly reduced (increased), implying GuCl bulk doping facilitating the crystallization of perovskite. New peak, which is not observed in the control and 3D films, is clearly observed at q = 8.3 nm^{-1} in the 2D/3D films. It is evident that guanidine halide can react with excess PbI_2 from the underlying 3D perovskite during the post-treatment process and form a capping layer 2D perovskite on the surface.[35,59] Therefore, we deduce that the newly formed 2D perovskites passivated the surface/interfacial defects, which are usually found in 3D perovskites, and formed a coherent interface for efficient hole transport and thus minimize the energy loss.[11,25]

To further confirm the crystalline of 2D/3D perovskite film, HAADF-STEM, SABD, and NBD has been carried out. With a view to the cross-section HAADF-STEM images of the dual optimization device (2D/3D), the representative spot diffractions (red circles) with the interplanar spacing of 3.13 and 6.78 Å, which are well matched with the (020) of $FAPbI_3$ and (040) of Gu_2PbI_4 (Figure 5d,e).[60] The introduction of interlayer dopants (GuI) widened the interplanar spacing, resulting in the formation Gu_2PbI_4 of (040) crystal planes with a wider d-spacing of 6.78 Å, which is consistent with NBD results (detailed experimental results as shown in Figures S15 and S16, Supporting Information).[8] In addition, NBD results show that $FAPbI_3$ layers with various crystallographic orientations, which suggest 3D perovskite belonged to polycrystalline film. And representative spot diffractions belong to (040) crystal planes of Gu_2PbI_4 on the 3D perovskite top surface. In brief, we have verified that guanidine halide treatment can facilitate crystallinity, improve the surface morphology, and form the 2D/3D hybrid film structure, which benefit to suppress the non-radiative recombination, confirmed by following defect characterization.

2.4. Defect Characterization

To study the dynamics of the photogenerated carriers, time resolved photoluminescence (TRPL) spectroscopy has been carried out. The result shows the increase in the carrier lifetime by applying guanidine halide treatment from 1.97 (control) to 2.52 and 3.18 μs (3D and 2D/3D) (**Figure 6**a). This indicates guanidine halide treatment can bring a high quality of perovskite crystal with low defect density, which reduces the defect-induced SRH recombination.[49,61] To further elucidate the mechanism for the enhancement of V_{oc}, capacitance–voltage (C–V) measurements were carried out. As illustrated in Figure S17, Supporting Information, the built-in potentials (V_{bi}) of control, 3D and 2D/3D device calculated by the corresponding Mott–Schottky curve are 0.94, 0.96, and 1.02 V. The higher V_{bi} implies stronger electric field in the PSCs which is beneficial for charge carrier separation and collection, resulting in the enhancement V_{oc}.[50] Space charge limited current (SCLC) analysis based on electron-only devices with the structure of $ITO/SnO_2/PVSK/PC_{61}BM/Au$ was carried out to estimate the electron trap density (Figure 6b). Based on the space charge limit current theory,[62] we can quantify that the defect density of control, 3D and 2D/3D device was 2.24×10^{15}, 1.37×10^{15}, and 1.24×10^{15} cm^{-3}, respectively. In addition, as shown in

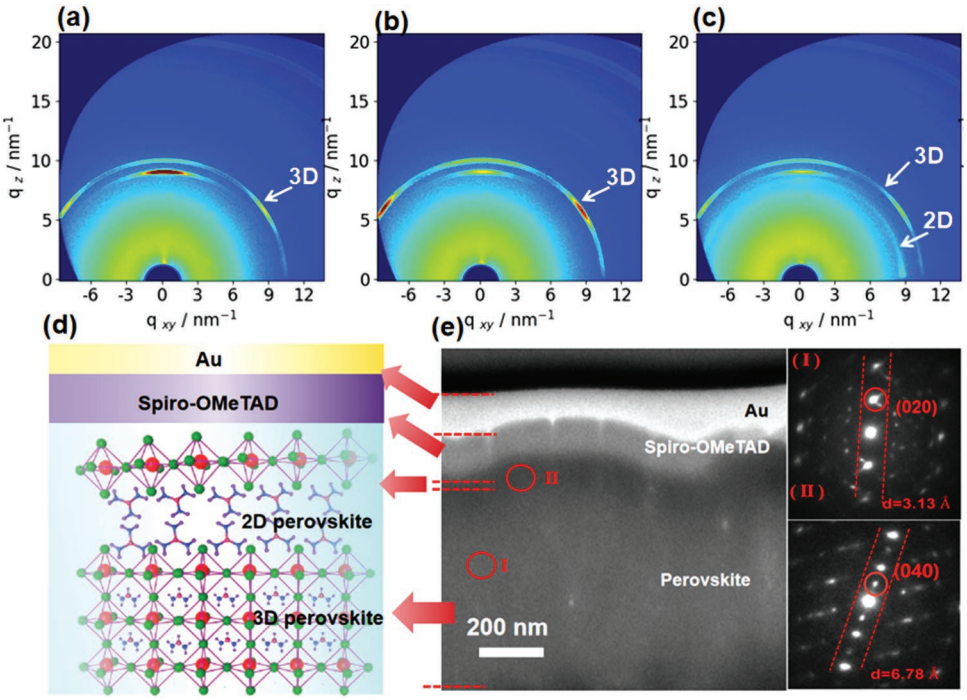

Figure 5. a–c) Wide-angle grazing incidence X-ray scattering (GIWAXS) of perovskite film. Structure diagram (d) cross-section high-angle annular dark-field scanning transmission electron microscopy result of (e); insets I and II show the corresponding NBD patterns of the red circle regions.

Figure 6c, the ideality factor of control device was fitted to be 1.95 via light power dependence V_{oc}, indicating serious SRH recombination.[52,63] By contrast, after the perovskite layer was passivated, the ideality factor reduced to 1.71 and 1.41 for 3D and 2D/3D device, respectively, indicating that the SRH recombination was effectively suppressed due to the defect passivation at the grain boundaries and surface. Meanwhile, electrochemical impedance spectroscopy (Figure S18 and Table S3, Supporting Information) shows an enhancement lifetime from 2.46 to 5.31 µs after the guanidine halide treatment, where lifetime can be extracted from high-frequency semicircle.[64] Both bulk and interface recombination resistance show obvious increase, suggesting that the guanidine halide treatment can effectively passivate the defect, which is consistent with above results.

Meanwhile, drive-level capacitance profiling (DLCP) have been employed to study the spatial distributions of defect states. The DLCP measurements have been performed on the control, 3D, and 2D/3D device at ac frequency of 10 kHz by subtracting the free carrier density measured at high ac frequencies (100 kHz). The acquired spatial distribution of the trap density is shown in Figure 6d. According to the defect analysis via DLCP, in the control device without GuX passivation, the defect densities are much larger at perovskite surface than those inside the perovskite bulk (4×10^{14} cm^{-3}), one surface is near the SnO_2/perovskite interface (10^{18} cm^{-3}) and the other is at perovskite/Spiro-OMeTAD interface (6.5×10^{16} cm^{-3}). By contrast, when GuCl is added to the bulk perovskite precursor, these buried interface and bulk defects are efficiently passivated, which are 6×10^{17} and 2.7×10^{14} cm^{-3} respectively. It indicates that GuCl can passivate buried interface as well as bulk perovskite, which is consistent with the previous reports.[35,36] The grain and interface are the place where defects are most easily formed. Therefore, we believe that the reduced bulk defect can mainly attribute to passivate the defect at the grain boundary.[56] Meanwhile, the interface tarp density near the perovskite/Spiro-OMeTAD of control and 3D is much larger than that of 2D/3D (1.4×10^{16} cm^{-3}), which results in the fact that GuI interface treatment can efficiently inhibit the formation of surface dangling bends.

Here, thermal admittance spectroscopy spectra of PSCs without or with the guanidine halide treatment has been carried out to investigate the active energy (E_a) of ion migration, which is related to stability via mobile ions migrating into the functional layers and PCE via mobile ions acting as nonradiative recombination centers.[65,66] The E_a of the pristine, 3D, and 2D/3D devices is 0.271, 0.407, and 0.515 eV, respectively (Figure 6e and detailed calculation process as shown in Figure S19, Supporting Information). The increased E_a indicates that the ion migration is suppressed significantly after the GuCl doping treatment and GuI surface modification. The increased E_a can be attributed to the fact that 1) GuCl doping in the perovskite layer facilitate crystallinity as predicted by our theoretical calculations as well as the XRD and SEM results, 2) GuI coating on the perovskite layer fills the iodine vacancies on the surface, confirmed by DLCP results. Meanwhile, GuI coating on the perovskite layer leads to the formation of the stable hydrophobic 2D (Gu_2PbI_4) perovskite on the perovskite top surface, resulting in the enhancement of the device stability.

2.5. Device stability

Organic–inorganic halide perovskites are highly sensitive to moisture and can be decomposed readily in a high-humidity

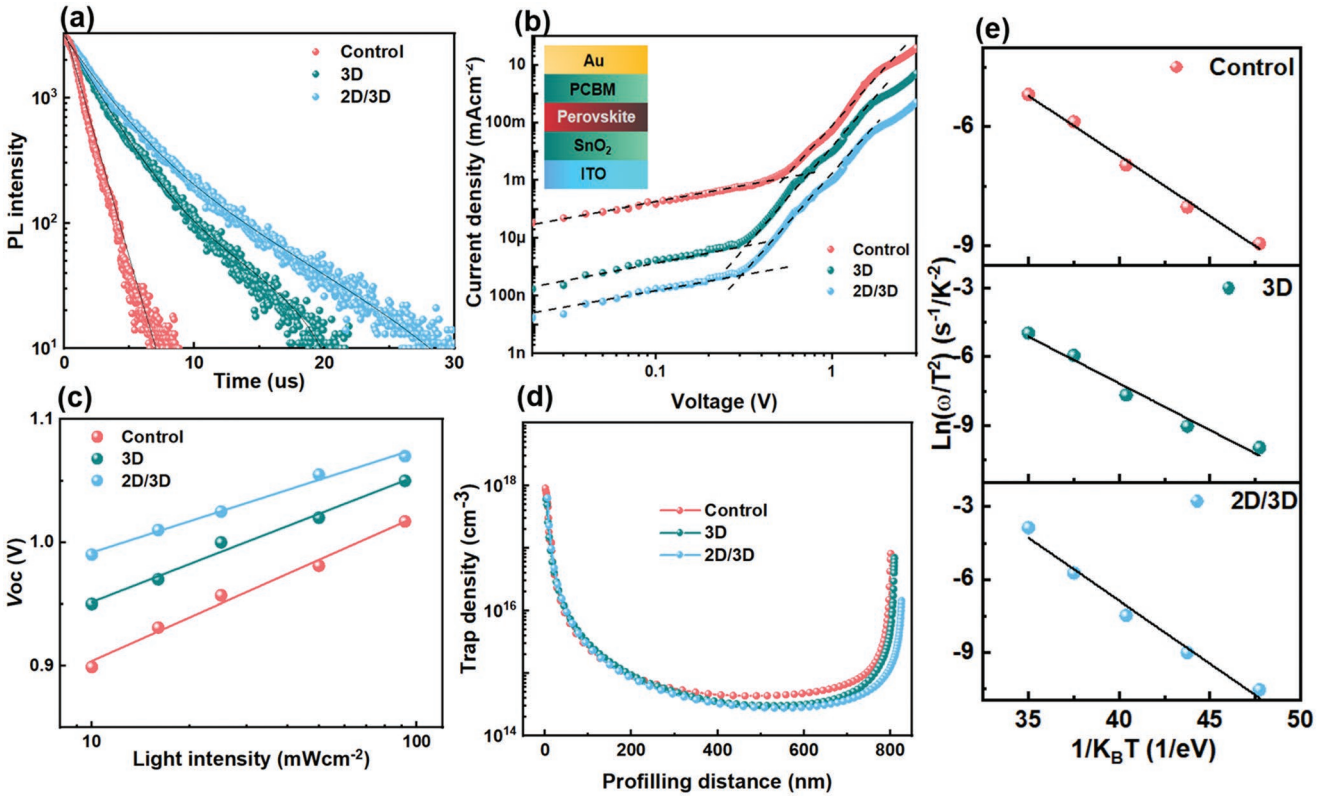

Figure 6. a) Time-resolved photoluminescence (TRPL) spectra for the perovskite films deposited on ITO glass. b) Capacitance–voltage (*C–V*) plots for all samples measured at 1000 Hz in dark. c) Dark *J–V* curves of the electron-only devices based on the perovskite film with or without the guanidine halide treatment. Inset: structure of the electron-only device. d) Relationship between V_{oc} and light intensity for different devices. d) Spatial distribution of defects of the PSCs for different devices via DLCP measurement. e) The corresponding Arrhenius plots of the characteristic frequencies to calculate the defect activation energy (E_a) of ion migration (from control, 3D, and 2D/3D device).

environment. In order to examine the water-resistant performance of perovskite with the guanidine halide treatment, we first measured the static water contact angles on the surface of control, 3D, and 2D/3D perovskite film (Figure S20, Supporting Information). The pristine perovskite film exhibits a smaller water contact angle (50°), compared with the 3D film (73°) and 2D/3D film (86°), which indicates the GuCl-incorporated and GuI surface treatment can improve the moisture stability. Meanwhile, the moisture stability of the PSCs without encapsulation was studied by exposing them in an ambient and dark environment for 30 days (relative humidity about 20%). We notice the PCE of GuCl-incorporated and GuI surface post-treated PSCs exhibit an excellent stability with a much slower degradation rate and retain > 90% of its initial value, compared to the pristine one which has shown a faster decrease which conserves only 78% of its initial value after storage of 30 days (**Figure 7**a). After the encapsulation, all devices are tested under the high relative humidity of 75% ± 5%, dark and ambient condition. As shown by Figure 7b, the final PCE of the pristine device is only 36% of its initial value. By contrast, the 3D and 2D/3D device can maintain about 80% of its initial PCE after 30 days. As reported, the defects at perovskite surface and grain boundaries are one of the main reasons for the accelerated moisture infiltration into perovskite layer.[61,67,68] The enhanced stability of the 3D and 2D/3D devices is mainly attributed to the efficient defect passivation as well as the robust moisture resistance at the perovskite surface and grain boundaries with the assistance of the guanidine halide treatment.

The light soaking stability was also monitored under a white LED lamp continuous illumination, open-circuit condition, and N2 environment for the different devices without encapsulation. The 2D/3D device also outperforms the control device under continuous illumination (Figure 7c). For the 2D/3D (3D) device, the efficiency dropped less than 20% (35%) after 30 days of illumination. By contrast, the control device showed severely deteriorated light stability after merely 20 days of illumination. The considerable improvement in light stability of 2D/3D device can be attributed to multi-functions of guanidine halide, revealing better quality of the film, ultra-hydrophobic nature, and suppression ions migration as confirmed by SEM, contact angle, and thermal admittance spectroscopy. Moreover, the presence of defects (especially grain boundaries and interface), which can effectively passivate by guanidine halide may provide a favorable pathway for the ion/metal migration causing degradation.[53] To understand which component of the guanidine halide (Gu^+ or X^-) is essential to improve the device's stability, we attempted either replacing the I^- anions with Br^- or Cl^- or replace Gu^+cation with PEA^+. Our results show that both replacements would result in obvious drop in the device stabilities (Figure 7d). Namely, both Gu^+ and I^- are required

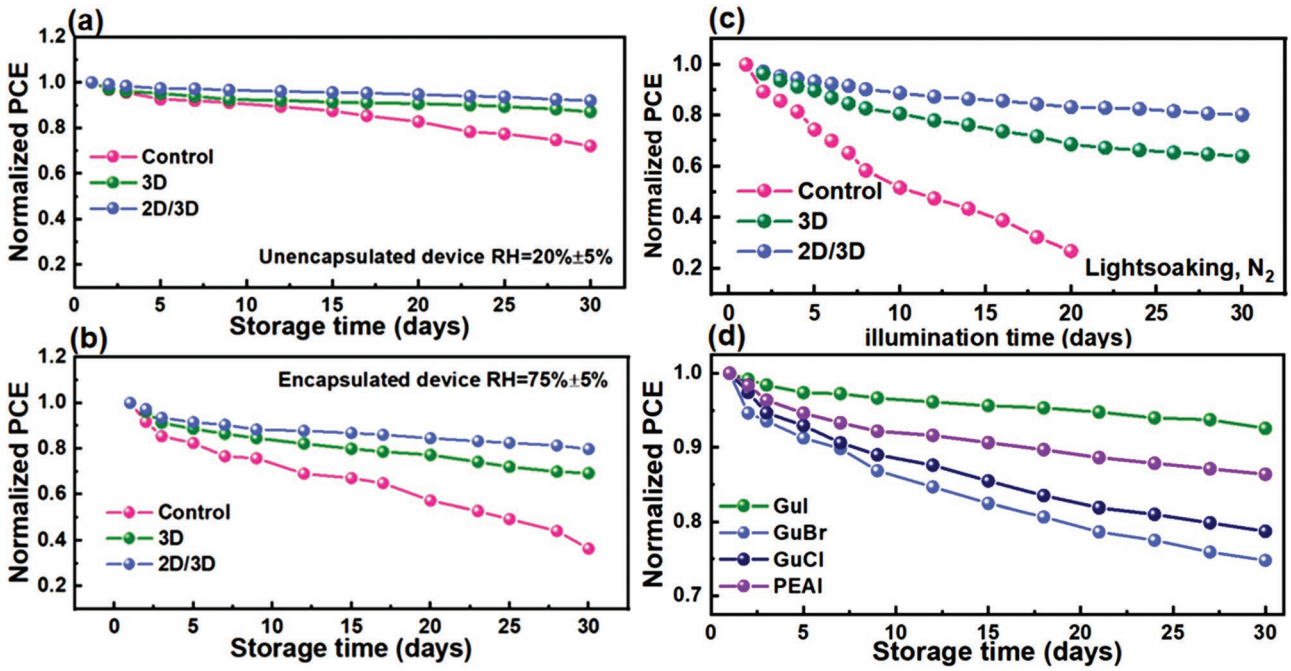

Figure 7. a) Stability of the unencapsulated perovskite solar cells performed under ambient air conditions. b) Stability of the encapsulated perovskite solar cells performed under RH = 75% conditions. c) Normalized PCEs of devices after continuous illumination for 30 days under N_2 environment. d) Stability of PSCs treated with different organic salts.

to improve the perovskite stability because of the formation of stable hydrophobic 2D perovskite and the passivation of iodine vacancy.

3. Conclusions

In this work, we realized a 2D/3D hybrid perovskite film to enhance both efficiency and stability, based on dual (bulk- and surface-) guanidine halide treatment passivation approach. It lowered the charge carrier losses in bulk perovskites and extended long-term stability by preventing surface structural decomposition. By combining with quantum chemistry calculations, Urbach energy and time-dependent photovoltage measurements, the engineered components of GuX salts are GuCl for bulk treatment and GuI surface treatment, respectively. The former suppressed nonradiative recombination, and the latter enhanced the stability by preventing from the halogen-out. Following the dual passivation approach, the 2D/3D hybrid perovskite film configuration was successfully realized, as confirmed by photoluminescence, X-ray diffraction, microstructure characterization, and electron diffraction. The defects were successfully passivated, which were confirmed by the time-dependent photocurrent measurement techniques. In the end, the 3D/2D perovskites achieved long-term stability (efficiency degradation <10% after 30 days without encapsulation) and much higher efficiency (22.53%) comparing with the efficiency (20.31%) of the control device. We provided a feasible approach to realize both high efficiency and long-term stability and a rational design strategy for bulk and surface treatment of the perovskite film.

Supporting Information

Supporting Information is available from the Wiley Online Library or from the author.

Acknowledgements

X.Z. and W.Z. contributed equally to this work. This work was supported by the National Science Foundation of China under Grant (No. 62034001, 61974008, 61922005, 52073005, 22033006), the Beijing Municipal Natural Science Foundation (Grant Nos. JQ20027, 4222065), the NSAF Joint Fund (No. U1930105), the General Program of Science and Technology Development Project of Beijing Municipal Education Commission (Grant No. KM202010005005), and the National Key Research and Development Program of China (2021YFA0715602). A portion of this work is based on the data obtained at BSRF-1W1A. The authors gratefully acknowledge the cooperation of the beamline scientists at BSRF-1W1A beamline.

Conflict of Interest

The authors declare no conflict of interest.

Data Availability Statement

The data that support the findings of this study are available from the corresponding author upon reasonable request.

Keywords

defect passivation, perovskite solar cells, stability

Received: March 30, 2022
Revised: May 3, 2022
Published online:

[1] A. Kojima, K. Teshima, Y. Shirai, T. Miyasaka, *J. Am. Chem. Soc.* **2009**, *131*, 6050.
[2] National Renewable Energy Laboratory, Best research-cell efficiencies chart, https://www.nrel.gov/pv/cell-efficiency.html.
[3] Y. Chen, Q. Meng, Y. Xiao, X. Zhang, J. Sun, C. B. Han, H. Gao, Y. Zhang, Y. Lu, H. Yan, *ACS Appl. Mater. Interfaces* **2019**, *11*, 44101.
[4] J. Chen, J.-Y. Seo, N.-G. Park, *Adv. Energy Mater.* **2018**, *8*, 1702714.
[5] G. Grancini, C. Roldán-Carmona, I. Zimmermann, E. Mosconi, X. Lee, D. Martineau, S. Narbey, F. Oswald, F. De Angelis, M. Graetzel, M. K. Nazeeruddin, *Nat. Commun.* **2017**, *8*, 15684.
[6] C. Liang, D. Zhao, P. Li, B. Wu, H. Gu, J. Zhang, T. W. Goh, S. Chen, Y. Chen, Z. Sha, G. Shao, T. C. Sum, G. Xing, *Nano Energy* **2019**, *59*, 721.
[7] Y. Liu, S. Akin, L. Pan, R. A. Uchida, J. V. H. M. Neha, F. S. Alexander, A. R. Z. Uhl, M. Shaik, A. D. Hagfeldt, M. Ibrahim, M. Grätze, *Sci. Adv.* **2019**, *5*, eaaw2543.
[8] G. Li, J. Song, J. Wu, Z. Song, X. Wang, W. Sun, L. Fan, J. Lin, M. Huang, Z. Lan, P. Gao, *ACS Energy Lett.* **2021**, *6*, 3614.
[9] A. A. Maxim, S. N. Sadyk, D. Aidarkhanov, C. Surya, A. Ng, Y. H. Hwang, T. S. Atabaev, A. N. Jumabekov, *Nanomaterials* **2020**, *10*, 291.
[10] B. Chen, P. N. Rudd, S. Yang, Y. Yuan, J. Huang, *Chem. Soc. Rev.* **2019**, *48*, 3842.
[11] S. Jeong, S. Seo, H. Yang, H. Park, S. Shin, H. Ahn, D. Lee, J. H. Park, N. G. Park, H. Shin, *Adv. Energy Mater.* **2021**, *11*, 2102236.
[12] H. Min, M. Kim, S.-U. Lee, H. Kim, G. Kim, K. Choi, J. H. Lee, S. I. Seok, *Science* **2019**, *366*, 749.
[13] Y. Zhang, Y. Li, L. Zhang, H. Hu, Z. Tang, B. Xu, N. G. Park, *Adv. Energy Mater.* **2021**, *11*, 2102538.
[14] F. Wang, Z. Wang, W. Sun, Z. Wang, Y. Bai, T. Hayat, A. Alsaedi, Z. Tan, *Small* **2020**, *16*, 2002940.
[15] Z. Wang, F. Wang, W. Sun, R. Ni, S. Hu, J. Liu, B. Zhang, A. Alsaed, T. Hayat, Z. A. Tan, *Adv. Funct. Mater.* **2018**, *28*, 1804187.
[16] Z. Wang, F. Wang, B. Zhao, S. Qu, T. Hayat, A. Alsaedi, L. Sui, K. Yuan, J. Zhang, Z. Wei, Z. Tan, *J. Phys. Chem. Lett.* **2020**, *11*, 1120.
[17] H. D. Pham, L. Xianqiang, W. Li, S. Manzhos, A. K. K. Kyaw, P. Sonar, *Energy Environ. Sci.* **2019**, *12*, 1177.
[18] D. Sirbu, F. H. Balogun, R. L. Milot, P. Docampo, *Adv. Energy Mater.* **2021**, *11*, 2003877.
[19] L. Mao, C. C. Stoumpos, M. G. Kanatzidis, *J. Am. Chem. Soc.* **2018**, *141*, 1171.
[20] G. Grancini, M. K. Nazeeruddin, *Nat. Rev. Mater.* **2018**, *4*, 4.
[21] P. Gao, A. B. Bin Mohd Yusoff, M. K. Nazeeruddin, *Nat. Commun.* **2018**, *9*, 5028.
[22] A. Krishna, S. Gottis, M. K. Nazeeruddin, F. Sauvage, *Adv. Funct. Mater.* **2018**, *29*, 1806482.
[23] X. Zhao, T. Liu, Y. L. Loo, *Adv. Mater.* **2021**, *34*, 2105849.
[24] X. Gu, W. Xiang, Q. Tian, S. F. Liu, *Angew. Chem.* **2021**, *133*, 23348.
[25] H. Kim, S. U. Lee, D. Y. Lee, M. J. Paik, H. Na, J. Lee, S. I. Seok, *Adv. Energy Mater.* **2019**, *9*, 1902740.
[26] J.-H. Kim, S.-G. Kim, N.-G. Park, *ACS Energy Lett.* **2021**, *6*, 3435.
[27] D. Lin, T. Zhang, J. Wang, M. Long, F. Xie, J. Chen, B. Wu, T. Shi, K. Yan, W. Xie, P. Liu, J. Xu, *Nano Energy* **2019**, *59*, 619.
[28] C. Liu, Y. Yang, K. Rakstys, A. Mahata, M. Franckevicius, E. Mosconi, *Nat. Commun.* **2021**, *12*, 6394.
[29] B. Yang, J. Suo, F. Di Giacomo, S. Olthof, D. Bogachuk, Y. Kim, X. Sun, *ACS Energy Lett.* **2021**, *6*, 3916.
[30] T. Zhou, H. Lai, T. Liu, D. Lu, X. Wan, X. Zhang, Y. Liu, Y. Chen, *Adv. Mater.* **2019**, *31*, 1901242.
[31] R. D. Chavan, D. Prochowicz, M. M. Tavakoli, P. Yadav, C. K. Hong, *Adv. Mater. Interfaces* **2020**, *7*, 2000105.
[32] Y. Zhang, P. Wang, M. C. Tang, D. Barrit, W. Ke, J. Liu, T. Luo, Y. Liu, T. Niu, D. M. Smilgies, Z. Yang, Z. Liu, S. Jin, M. G. Kanatzidis, A. Amassian, S. F. Liu, K. Zhao, *J. Am. Chem. Soc.* **2019**, *141*, 2684.
[33] S. Wu, Z. Li, J. Zhang, T. Liu, Z. Zhu, A. K. Jen, *Chem. Commun.* **2019**, *55*, 4315.
[34] Z. Li, L. L. Hao, Dachang, X. S. , Q. Zhao, Z. Shao, C. Chen, X. Wang, L. Wang, G. Cui, S. Pang, *Solar RRL.* **2022**, *2200003*.
[35] B. Chen, H. Chen, Y. Hou, J. Xu, S. Teale, K. Bertens, H. Chen, A. Proppe, Q. Zhou, D. Yu, K. Xu, M. Vafaie, Y. Liu, Y. Dong, E. H. Jung, C. Zheng, T. Zhu, Z. Ning, E. H. Sargent, *Adv. Mater.* **2021**, *33*, 2103394.
[36] Y. Zhang, Y. Wang, L. Zhao, X. Yang, C.-H. Hou, J. Wu, R. Su, S. Jia, J.-J. Shyue, D. Luo, P. Chen, M. Yu, Q. Li, L. Li, Q. Gong, R. Zhu, *Energy Environ. Sci.* **2021**, *14*, 6526.
[37] P. Wang, B. Chen, R. Li, S. Wang, N. Ren, Y. Li, S. Mazumdar, B. Shi, Y. Zhao, X. Zhang, *ACS Energy Lett.* **2021**, *6*, 2121.
[38] M. Abuhelaiqa, S. Paek, Y. Lee, K. T. Cho, S. Heo, E. Oveisi, A. J. Huckaba, H. Kanda, H. Kim, Y. Zhang, R. Humphry-Baker, S. Kinge, A. M. Asiri, M. K. Nazeeruddin, *Energy Environ. Sci.* **2019**, *12*, 1910.
[39] W. Hui, Y. Yang, Q. Xu, H. Gu, S. Feng, Z. Su, M. Zhang, J. Wang, X. Li, J. Fang, F. Xia, Y. Xia, Y. Chen, X. Gao, W. Huang, *Adv. Mater.* **2019**, *32*, 1906374.
[40] X. Shi, Y. Ding, S. Zhou, B. Zhang, M. Cai, J. Yao, L. Hu, J. Wu, S. Dai, M. K. Nazeeruddin, *Adv. Sci.* **2019**, *6*, 1901213.
[41] B. Tu, Y. Shao, W. Chen, Y. Wu, X. Li, Y. He, J. Li, F. Liu, Z. Zhang, *Adv. Mater.* **2019**, *31*, 1805944.
[42] Y. Zhang, X. Liu, P. Li, Y. Duan, X. Hu, F. Li, Y. Song, *Nano Energy* **2019**, *56*, 733.
[43] J. He, W. H. Fang, R. Long, O. V. Prezhdo, *J. Am. Chem. Soc.* **2020**, *142*, 14664.
[44] W. Li, Y. Y. Sun, L. Li, Z. Zhou, J. Tang, O. V. Prezhdo, *J. Am. Chem. Soc.* **2018**, *140*, 15753.
[45] R. Long, J. Liu, O. V. Prezhdo, *J. Am. Chem. Soc.* **2016**, *138*, 3884.
[46] B. W. Park, S. I. Seok, *Adv. Mater.* **2019**, *31*, 1805337.
[47] R. Hidayat, A. A. Nurunnizar, A. Fariz, Herman, E. S. Rosa, Shobih, T. Oizumi, A. Fujii, M. Ozaki, *Sci. Rep.* **2020**, *10*, 19197.
[48] T. Liu, J. Guo, D. Lu, Z. Xu, Q. Fu, N. Zheng, Z. Xie, X. Wan, X. Zhang, Y. Liu, Y. Chen, *ACS Nano* **2021**, *15*, 7811.
[49] G. Kim, H. Min, K. S. Lee, S. M. Yoon, S. I. Seok, *Science* **2020**, *370*, 108.
[50] P. Wang, R. Li, B. Chen, F. Hou, J. Zhang, Y. Zhao, X. Zhang, *Adv. Mater.* **2020**, *32*, 1905766.
[51] Y. Bai, S. Xiao, C. Hu, T. Zhang, X. Meng, H. Lin, Y. Yang, S. Yang, *Adv. Energy Mater.* **2017**, *7*, 1701038.
[52] J. Yao, H. Wang, P. Wang, R. S. Gurney, A. Intaniwet, P. Ruankham, S. Choopun, D. Liu, T. Wang, *Mater. Chem. Front.* **2019**, *3*, 1357.
[53] W. Zhang, J. Xiong, J. Li, W. A. Daoud, *J. Mater. Chem. A* **2019**, *7*, 9486.
[54] X. Xiao, W. Zhang, W. Zhang, J. Du, C. Zhang, G. Xu, A. Mei, Y. Rong, Y. Hu, H. Han, *Chem. Mater.* **2022**, *34*, 2231.
[55] M. K. Kim, G.-H. Kim, T. K. Lee, I. W. Choi, H. W. Choi, Y. Jo, Y. J. Yoon, J. W. Kim, J. Lee, D. Huh, S. K. Kwak, J. Y. Kim, D. S. Y. Kim, C. D. Kim, *Joule* **2019**, *3*, 2179.
[56] Q. Jiang, Y. Zhao, X. Zhang, X. Yang, Y. Chen, Z. Chu, Q. Ye, X. Li, Z. Yin, J. You, *Nat. Photonics* **2019**, *13*, 460.
[57] L. Gao, X. Li, Y. Liu, J. Fang, S. Huang, I. Spanopoulos, X. Li, Y. Wang, L. Chen, G. Yang, M. G. Kanatzidis, *ACS Appl. Mater. Interfaces* **2020**, *12*, 43885.
[58] M. Qin, H. Xue, H. Zhang, H. Hu, K. Liu, Y. Li, Z. Qin, J. Ma, H. Zhu, K. Yan, *Adv. Mater.* **2020**, *32*, 2004630.
[59] F. C. Zhang, B. Cai, J. Song, B. Han, B. Zhang, H. Zeng, *Adv. Funct. Mater* **2020**, *30*, 2001732.
[60] T. W. Kim, S. Uchida, T. Matsushita, L. Cojocaru, R. Jono, K. Kimura, D. Matsubara, M. Shirai, K. Ito, H. Matsumoto, T. Kondo, H. Segawa, *Adv. Mater.* **2018**, *30*, 1705230.
[61] K. Liu, Q. Liang, M. Qin, D. Shen, H. Yin, Z. Ren, Y. Zhang, H. Zhang, P. W. K. Fong, Z. Wu, J. Huang, J. Hao, Z. Zheng, S. K. So, C.-S. Lee, X. Lu, G. Li, *Joule* **2020**, *4*, 2404.
[62] J. Chen, N. G. Park, *Adv. Mater.* **2018**, *31*, 1803019.

[63] F. Li, J. Zhang, S. Jo, M. Qin, Z. Li, T. Liu, X. Lu, Z. Zhu, A. K. Y. Jen, *Small Methods* **2020**, *4*, 1900831.
[64] X. Chen, Y. Shirai, M. Yanagida, K. Miyano, *J. Phys. Chem. C* **2019**, *123*, 3968.
[65] X. Zhang, X. Chen, Y. Chen, N. A. Nadege Ouedraogo, J. Li, X. Bao, C. B. Han, Y. Shirai, Y. Zhang, H. Yan, *Nanoscale Adv.* **2021**, *3*, 6128.
[66] C. Tong, L. Li, L. Liu, O. V. Prezhdo, *J. Am. Chem. Soc.* **2020**, *142*, 3060.
[67] N. A. N. Ouedraogo, Y. Chen, X. Zhang, H. Yan, C. B. Han, Y. Zhang, *Sustainable Energy Fuels* **2020**, *4*, 4257.
[68] Q. Wang, B. Chen, Y. Liu, Y. Deng, Y. Bai, Q. Dong, J. Huang, *Energy Environ. Sci.* **2017**, *10*, 516.